AIAA JOURNAL
Vol. 49, No. 10, October 2011

Study on the Chaotic Dynamics in Attitude Maneuver of Liquid-Filled Flexible Spacecraft

Bao-Zeng Yue*
Beijing Institute of Technology, 100081 Beijing, People's Republic of China

DOI: 10.2514/1.J050144

In this paper, the chaotic dynamics in an attitude transition maneuver of a coupled slosh–spacecraft with a flexible appendage in going from minor axis to major axis spin under the influence of dissipative effects due to fuel slosh and a small flexible appendage constrained to undergo only torsional vibration is investigated. The coupled slosh–spacecraft with a flexible appendage in attitude maneuver carrying a sloshing liquid is considered a multibody system with the sloshing motion modeled as a spherical pendulum. The focus in this paper is on the way in which the dynamics of the liquid and the flexible appendage vibration are coupled. The equations of motion are derived and then transformed into a form suitable for the application of the Melnikov method. The Melnikov integral is used to predict the transversal intersections of the stable and unstable manifolds for the perturbed system. An analytical criterion for chaotic motion is derived in terms of the system parameters. This criterion is evaluated for its significance to the design of spacecraft. The dependence of the onset of chaos on quantities such as body shape and magnitude of damping values, fuel fraction, and torsional vibration frequency of the flexible appendage are investigated. In addition, extensive numerical simulations are carried out to check the range of validity of the Melnikov result.

Downloaded by University of Hong Kong Libraries on October 21, 2012 | http://arc.aiaa.org | DOI: 10.2514/1.J050144

Nomenclature

A, B, C	=	mass moment of inertia for appendage
a	=	elastic appendage
b	=	rigid carrier body
c	=	center of mass for entire system
C_θ, C_ϕ	=	viscous damping coefficient of fuel slosh
c_1	=	center of mass of appendage
d	=	distance from center of mass for appendage to center of mass for carrier body
$e_1e_2e_3$	=	coordinate frame attached to center of mass for entire system
G	=	shear modulus for connecting rod
h_i	=	angular momentum for spacecraft
I_1, I_2, I_3	=	mass moment of inertia for carrier body
K	=	torsional stiffness of connecting rod
L	=	length of elastic rod
l	=	length of pendulum arm
L_{TV}	=	Lagrangian for flexible-liquid–spacecraft coupled system
m	=	tip mass for appendage
m_f	=	bob mass of pendulum
O	=	pivot point of pendulum
r_i	=	nondimensional geometric parameter for spacecraft
S	=	polar area moment of inertia for connecting rod
T_1, T_2	=	kinetic energy of carrier body and appendage
V	=	potential energy of torsional rod
α	=	angle of twist for appendage
ε	=	perturbation parameter
$\zeta_1\zeta_2\zeta_3$	=	coordinate frame attached to center of mass for appendage
λ_i, G_1	=	nondimensional parameters of mass momentum of inertia for coupled system
τ	=	nondimensionalization of time t
ϕ, θ	=	circumferential and radial coordinates for pendulum
Ω	=	frequency of appendage oscillation
ω	=	angular velocity of carrier body

Received 19 August 2009; revision received 4 November 2010; accepted for publication 16 May 2011. Copyright © 2011 by the American Institute of Aeronautics and Astronautics, Inc. All rights reserved. Copies of this paper may be made for personal or internal use, on condition that the copier pay the $10.00 per-copy fee to the Copyright Clearance Center, Inc., 222 Rosewood Drive, Danvers, MA 01923; include the code 0001-1452/11 and $10.00 in correspondence with the CCC.

*Department of Mechanics, School of Aerospace Engineering.

I. Introduction

THE attitude evolution of a rigid body under various torques has been extensively studied over the past few decades because of its importance in aerospace engineering [1–11]. The determination and control of attitude evolution are important problems in modern spacecraft dynamics. It is well known that, for a torque-free rigid body with distinct moments of inertia, the rotations about the axes of maximum and minimum moments of inertia are stable (center) and the rotation about the axis of medium moment of inertia is unstable (saddle). When a rigid body is subject to a small torque, the heteroclinic orbits (separatrix) that connect the saddles are expected to break and, perhaps, to intersect transversely. The existence of transversal intersection of heteroclinic (homoclinic) orbits implies complex dynamic behavior in the sense of the Smale horseshoe and provides a necessary condition for chaotic motion to occur. There is an analytical technique, the Melnikov method, to detect the transversal intersections of heteroclinic (homoclinic) orbits and chaotic motion in nonlinear dynamic systems, using ideas that go back to Poincaré [12–15]. Because it is often important to be able to predict accurately the timing or sequence of attitude maneuver, and because the presence of chaotic dynamics could render useless any attempt at this prediction, it is important to be able to understand when chaos will play a role in the attitude dynamics of a spacecraft. The equations of motion describing the attitude dynamics of complex nonrigid spacecraft are readily derived, but their analytical solution is elusive. In fact, if the system is nonlinear, and thus potentially chaotic, these solutions are fundamentally unobtainable. On the other hand, solutions to these highly nonlinear equations can be obtained for specific parameter values using numerical simulation, but many interesting features of the dynamics can be lost in the numerical data. Fortunately, a great deal of physical insight into the behavior of these complex systems can be obtained by using a simpler rigid body with perturbations approximation for modeling and analyzing the spacecraft.

Certain aspects of the dynamics of attitude transition maneuvers have been studied for the special class of spacecraft called dual-spin satellites. These satellites are reoriented by spinup of rotors relative to the main spacecraft body. Attitude resonance in this maneuver, occurring during the spinup or spindown, has been investigated using

Downloaded by University of Hong Kong Libraries on October 21, 2012 | http://arc.aiaa.org | DOI: 10.2514/1.J050144

perturbation techniques and numerical simulation [1–5]. In the case of single-body satellites, the direction and control of the final major axis orientation have been studied by authors such as Barba et al. [6]. Recently, Gray et al. [16] and Miller and Gray [17] used the Melnikov method to detect the chaotic saddles of damped satellites subject to small perturbations due to small oscillating submass, a small flexible appendage constrained to undergo only torsional vibration, and a rotor immersed in a viscous fluid in an attitude transition maneuver. In their studies, the spherical coordinates were used to transform the equations of motion into a form suitable for the application of the Melnikov method, and the analytical criteria for chaotic motion to occur were derived in terms of the system parameters. The problem of the motion of a solid body with cavities completely filled with a liquid has been of major concern to aerospace engineers. Rumyantsev reviewed the motion stability of a rigid body with fluid-filled bodies [18]. The Lyapunov–Rumyantsev theorem is widely used in the design of artificial satellites and liquid-filled projectiles. Rahn modeled the spacecraft as a rigid body with a spherical, dissipative fuel slug, presenting a control system that guarantees a final orientation after spin transition [19]. Yue explored the chaotic dynamics in an attitude transition maneuver of a completely liquid-filled spacecraft under the influence of viscous damping and a small flexible appendage constrained to undergo only torsional vibration [20–22].

The study of liquid slosh in moving containers had been a problem of considerable interest, especially in modern spacecraft, which tend to carry reasonably large amounts of liquid fuel for injection from low Earth orbit to their final orbit, for stationkeeping and for precision attitude maneuvers. Depending on the frequency of the disturbance and the container shape, the free surface of the liquid will undergo a number of complex motions, including nonplanar, rotational, irregular beating, quasi periodic, and chaotic. In these cases, the energy dissipation due to sloshing of liquid fuel can be an important factor affecting spacecraft performance. Accurate models of liquid sloshing motion are therefore required to be able to predict the dynamics of fuel slosh and its influence on the overall dynamics of the spacecraft carrying the liquid fuel. A realistic representation of the liquid dynamics inside closed containers can be approximated by an equivalent mechanical system. The technique of equivalent mechanical models is a very useful mathematical tool for solving the complete dynamics problem of a system containing liquid. The new equivalent models approximated liquid sloshing as a mechanical system and appeared possible to be included into the spacecraft dynamics [23]. Determination of the parameters of the equivalent mechanical system is a difficulty and tricky business that requires improved slosh rigs and advanced methods of data analysis [24]. Rotary liquid slosh is one form of nonlinear response that has been recognized from spinning spacecraft, but because of its particular complexity, the hydrodynamic equations have never been formulated and solved. Rotary liquid slosh under harmonic excitation has been described by using a spherical pendulum model [25,26]. Many spinning spacecraft are unstable spinners and will enter a flat spin if the rotation is not controlled. The rotation growth is caused by energy dissipation resulting from fluid motions in the tanks, so it is important to quantify those motions. Abramson [27] and Dodge and Abramson [28] have also been leading all of this type of work at the Southwest Research Institute for at least a decade. In recent previous work, the chaotic attitude dynamics and the reorientation maneuver for completely viscous liquid-filled spacecraft with a flexible appendage were investigated, where the fuel was modeled as a spherical slug of inertia momentum J that is surrounded by a viscous layer. The chaotic attitude motions were revealed by numerical simulations, and the control strategy for the reorientation maneuver was designed to guarantee the desired final spin polarity [22].

In this paper, the chaotic dynamics in an attitude transition maneuver of a coupled slosh–spacecraft with a flexible appendage maneuvering from minor axis to major axis spin under the influence of dissipative effects due to fuel slosh and a small flexible appendage constrained to undergo only torsional vibration is investigated. The coupled slosh–spacecraft with a flexible appendage in attitude maneuver carrying a sloshing liquid is considered a multibody system with the sloshing motion modeled as a spherical pendulum. The focus in this paper is on the way in which the dynamics of the liquid and the flexible appendage vibration are coupled. The Melnikov method, developed for analyzing the slowly varying oscillator, is used to predict the transversal intersections of stable and unstable manifolds for the coupled dynamic multibody system of liquid slosh and flexible spacecraft. It is shown that there exist transversal intersections of heteroclinic orbits for certain parameter ranges. Thus, the attitude motion of liquid-filled spacecraft under the influence of a flexible appendage could become quite complex and may give rise to chaotic motions. The types of problems considered are not only of theoretic interest but also of practical importance in satellite design to avoid the occurrence of chaotic motion. For instance, the criterion obtained would be of great help in designing spinning satellites. In Sec. II, the mathematical equations are developed and the Melnikov function using the residue theory is derived. In Sec. III, the conditions for the existence of transverse homoclinic points are obtained, and the bifurcation to Smale's horseshoe is discussed. In Sec. IV, the chaotic attractors are turned to and studied numerically. In Sec. V are a few remarks with conclusions.

II. Mathematical Formulations

A. Spacecraft Model Description

The configuration of the coupled slosh–spacecraft system under consideration is shown in Fig. 1. The model consists of a rigid carrier body b, a partially liquid-filled spherical container, and an elastic appendage a. This model is assumed to be free of any external moments, such as gravity-gradient effects or atmospheric drag. An orthogonal coordinate frame, e_1, e_2, and e_3, is attached to c, the center of mass for the subsystem including the carrier body and the flexible appendage. The carrier and the liquid fuel have three components of the body mass moment of inertia, I_1, I_2, and I_3, about the major, intermediate, and minor body axes, respectively. Appendage a is modeled by a rigid-tip mass m joined to the carrier body by an elastic rod of length L and of negligible mass. The center of mass of the appendage a is located at c_1, a distance d along the e_1 axis. A second orthogonal coordinate frame, ζ_1, ζ_2, and ζ_3, is attached to the appendage at c_1 such that $\boldsymbol{e}_1$ and ζ_1 axes are collinear. For the appendage, the mass moment of inertia matrix with respect to the appendage coordinate frame, ζ_1, ζ_2, and ζ_3, is diag $\{A, B, C\}$. The fuel slosh is modeled as a spherical pendulum with the coordinate system designated in Fig. 2. Suppose the pivot point of the pendulum is located at point O (coinciding with mass center c_1 in Fig. 1), and l is the length of the massless rod connecting the pendulum bob of mass m_f. The tangential and radial angular displacement of the pendulum is defined by the generalized coordinates or angles φ and θ, shown in Fig. 2. Next, quantities describing the motion of the model will be introduced. The inertial angular velocity vector $\boldsymbol{\omega}$ of the carrier body b in the body-fixed reference frame is defined to be $\boldsymbol{\omega} = \omega_1\boldsymbol{e}_1 + \omega_2\boldsymbol{e}_2 + \omega_3\boldsymbol{e}_3$. The motion of the tip mass on the appendage is limited to rotation about the $\boldsymbol{e}_1$ axis and is defined by the angle of twist α. No flexural bending or warping of the connecting rod is permitted. This type of motion is

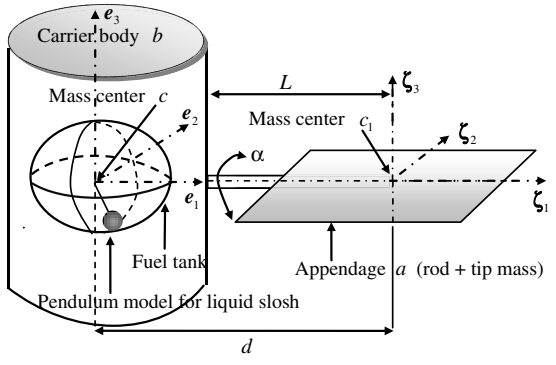

Fig. 1 Model of liquid-filled spacecraft with flexible appendage.

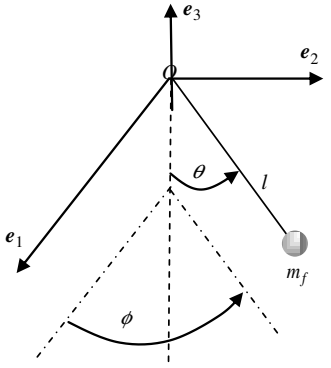

Fig. 2 Spherical pendulum model for fuel slosh.

possible if, for example, the appendage is constrained by a system of guy wires [17]. As a result, the motion of the appendage does not shift the center of the system. The connecting rod has a circular cross section and a torsional stiffness $K = SG/L$, where S is polar area moment of inertia, G is the shear modulus, and L is the length of the rod. The appendage can rotate at rate $\dot{\alpha}$ relative to the carrier body.

B. Equations of Motion

The kinetic energy of the carrier body and the fuel slosh is given by

$$T_1 = \tfrac{1}{2}I_1\omega_1^2 + \tfrac{1}{2}I_2\omega_2^2 + \tfrac{1}{2}\omega_3^2 + \tfrac{1}{2}m_f l^2[(\dot{\phi}\sin\theta + \omega_1\cos\theta\cdot\cos\phi + \omega_2\cos\theta\cdot\sin\phi + \omega_3\sin\theta)^2 + (\dot{\theta} + \omega_1\sin\phi - \omega_2\cos\phi)^2] \quad (1)$$

Since the gravitational effects are ignored, the potential energy for fuel slosh is assumed to be zero. The inertia matrix of the appendage is transformed so that its components are expressed in the body-fixed $\boldsymbol{e}_1$, $\boldsymbol{e}_2$, and $\boldsymbol{e}_3$ frame instead of the appendage-fixed ζ_1, ζ_2, and ζ_3 frame, and the kinetic energy is now derived to be

$$T_2 = \tfrac{1}{2}[A(\omega_1 + \dot{\alpha})^2 + B(\omega_2\cos\alpha + \omega_3\sin\alpha)^2 + C(\omega_3\cos\alpha - \omega_2\sin\alpha)^2 + m_a d^2(\omega_2^2 + \omega_3^2)] \quad (2)$$

The only component of the spacecraft that contributes to the potential energy is the torsional rod joining the carrier body to the tip mass of the appendage. This rod has torsional stiffness K; thus, its potential energy is given by

$$V = \tfrac{1}{2}K\alpha^2 \quad (3)$$

The fully coupled nonlinear Lagrangian for flexible-liquid–spacecraft motion is

$$L_{TV} = T_1 + T_2 + V \quad (4)$$

By applying the Lagrange equation to the resulting form of Eq. (4), the familiar Newton–Euler angular momentum relationship is obtained:

$$\dot{h}_1 = \omega_3 h_2 - \omega_2 h_3, \qquad \dot{h}_2 = \omega_1 h_3 - \omega_3 h_1$$
$$\dot{h}_3 = \omega_2 h_1 - \omega_1 h_2 \quad (5)$$

Because the phase space of the differential equations in terms of the angular momentum components is spherical rather than ellipsoidal, as it is in body angular velocity components, the angular velocity components are eliminated by computing $\boldsymbol{h} = \{\partial L/\partial\boldsymbol{\omega}\}$ to get angular momentum components in terms of angular velocity components, where $\{\partial L/\partial\boldsymbol{\omega}\}$ is the gradient vector of the Lagrangian with respect to the angular velocities $\boldsymbol{\omega}$. As such, the following relations between $\boldsymbol{h}$ and $\boldsymbol{\omega}$ are derived:

$$h_1 - m_f l^2\sin\phi\cdot\dot{\theta} - \tfrac{1}{2}m_f l^2\sin 2\theta\cdot\cos\phi\cdot\dot{\phi} - A\dot{\alpha} = (I_1 + m_f l^2\cos^2\theta + m_f l^2\sin^2\theta\cdot\sin^2\phi)\omega_1 - \tfrac{1}{2}m_f l^2\sin^2\theta\cdot\sin 2\phi\cdot\omega_2 + \tfrac{1}{2}m_f l^2\sin 2\theta\cdot\cos\phi\cdot\omega_3 \quad (6)$$

$$h_2 - m_f l^2\cos\phi\cdot\dot{\theta} - \tfrac{1}{2}m_f l^2\sin 2\theta\cdot\sin\phi\cdot\dot{\phi} - A\dot{\alpha} = -\tfrac{1}{2}m_f l^2\sin^2\theta\cdot\sin 2\phi\cdot\omega_1 + (I_2 + m_f l^2\cos^2\theta + m_f l^2\sin^2\theta\cdot\sin^2\phi + m_a d^2 + c\sin^2\alpha)\omega_2 + (\tfrac{1}{2}m_f l^2\sin 2\theta\cdot\sin\phi + \tfrac{1}{2}B\sin 2\alpha - \tfrac{1}{2}C\sin 2\alpha)\omega_3 \quad (7)$$

$$h_3 - m_f l^2\sin^2\theta\cdot\phi = \tfrac{1}{2}m_f l^2\sin 2\theta\cdot\cos\phi\cdot\omega_1 + (\tfrac{1}{2}m_f l^2\sin 2\theta\cdot\sin\phi + \tfrac{1}{2}B\sin 2\alpha - \tfrac{1}{2}C\sin 2\alpha)\omega_2 + (I_3 + m_f l^2\sin\theta^2 + B\sin^2\alpha + C\cos^2\alpha + m_a d^2)\omega_3 \quad (8)$$

Obviously, it is a tedious task to get the explicit hand-derived representations for ω_i because of the extreme complexity. The software MATLAB, however, can be used as an efficient tool in the numerical computational procedure to produce angular velocity from Eqs. (6–8). Substituting the obtained angular velocity into Eq. (5) will yield the equations of motion for the carrier body.

Attention is now turned to deriving the equation of motion for the flexible appendage. Rotation of the appendage relative to the carrier body is measured by the angle α, which is a generalized position coordinate of the system. The equation of motion for the appendage is given by the standard Lagrange equation relationship:

$$\frac{\mathrm{d}}{\mathrm{d}t}\frac{\partial L_{TV}}{\partial\dot{\alpha}} - \frac{\partial L_{TV}}{\partial\alpha} = 0 \quad (9)$$

Evaluating Eq. (9), the equation of motion for the appendage is attained:

$$A(\ddot{\alpha} + \dot{\omega}_1) - B(\omega_3\cos\alpha - \omega_2\sin\alpha)(\omega_2\cos\alpha + \omega_3\sin\alpha) + C(\omega_3\cos\alpha - \omega_2\sin\alpha)(\omega_2\cos\alpha + \omega_3\sin\alpha) + K\alpha = 0 \quad (10)$$

In a similar way, the equations of motion for the fuel slosh can be derived:

$$\ddot{\theta} + \frac{c_\theta}{m_f l^2}\dot{\theta} + [(\omega_1\cos\phi + \omega_2\sin\phi)(1 - \cos 2\theta) - \omega_3\sin 2\theta]\dot{\phi} - \frac{1}{2}\sin 2\theta\cdot\dot{\phi}^2 + \sin\phi\cdot\dot{\omega}_1 - \cos\phi\cdot\dot{\omega}_2 - \cos 2\theta\cdot(\omega_1\omega_2\sin 2\phi + \omega_2\omega_3\sin\phi) + \frac{1}{2}\sin 2\theta[(\omega_1\cos\phi + \omega_2\sin\phi)^2 - \omega_3^2] = 0 \quad (11)$$

$$\ddot{\phi}\sin^2\theta + \left(\dot{\theta}\sin 2\theta + \frac{c_\phi}{m_f l^2}\right)\dot{\phi} + [(\omega_1\cos\phi + \omega_2\sin\phi)\times(\cos 2\theta - 1) + \omega_3\sin 2\theta]\dot{\theta} + \frac{\dot{\omega}_1}{2}\sin 2\theta\cdot\cos\phi + \frac{\dot{\omega}_2}{2}\sin 2\theta\cdot\sin\phi + \dot{\omega}_3\sin^2\theta + \omega_1\omega_2\cos 2\phi\cdot\sin^2\theta + \left(\frac{\omega_2^2}{2} - \frac{\omega_1^2}{2}\right)\sin 2\phi\cdot\sin^2\theta + \frac{\omega_1\omega_3}{2}\sin 2\theta\cdot\sin\phi - \frac{\omega_2\omega_3}{2}\sin 2\theta\cdot\cos\phi = 0 \quad (12)$$

where C_θ, C_ϕ is the viscous damping coefficient of the fuel slosh. The angular velocities ω_1, ω_2, and ω_3 in Eqs. (10–12) can be replaced by angular momenta through Eqs. (6–8) to obtain the equations of motion for the appendage and pendulum in terms of body angular momenta. Equations (5) and (10–12) govern the dynamics of the overall system.

Downloaded by University of Hong Kong Libraries on October 21, 2012 | http://arc.aiaa.org | DOI: 10.2514/1.J050144

Downloaded by University of Hong Kong Libraries on October 21, 2012 | http://arc.aiaa.org | DOI: 10.2514/1.J050144

C. Nondimensionalization of the Equations of Motion

It is now convenient to nondimensionalize the equations of motion and explicitly introduce the perturbation parameter ε. This makes clearer which terms are small, and therefore higher order, and which terms are to be retained. To do this, the following assumptions about the relative size of the system parameters are made:

$$A = O(\varepsilon), \qquad B = O(\varepsilon), \qquad C = O(\varepsilon), \qquad C - B = O(\varepsilon^2)$$
$$K = O(\varepsilon), \qquad \dot{\theta} = O(\sqrt{\varepsilon}), \qquad \dot{\phi} = O(\sqrt{\varepsilon}) \qquad md^2 = O(\varepsilon)$$

Then, the following rescaled quantities are defined:

$$\varepsilon \underline{\Delta} \frac{m_f l^2}{I_2}, \qquad \tau = \frac{ht}{I_2}, \qquad \tilde{h}_i = \frac{h_i}{h}, \qquad \tilde{h}_i' \underline{\Delta} \left(\frac{I_2}{h^2}\right) \dot{h}_i$$
$$r_1 \underline{\Delta} \frac{I_3}{I_2} > 1, \qquad r_2 \underline{\Delta} \frac{I_1}{I_2} < 1, \qquad \lambda \underline{\Delta} \frac{A}{m_f l^2}, \qquad r_3 \underline{\Delta} \frac{A}{B}$$
$$\tilde{K} \underline{\Delta} \frac{K I_2}{h^2 \varepsilon}, \qquad \tilde{\Omega} \underline{\Delta} \frac{\Omega I_2}{h}, \qquad G_1 \underline{\Delta} \frac{B}{md^2}, \qquad \tilde{\omega}_i \underline{\Delta} \frac{I_2 \omega_i}{h}$$
$$\tilde{C}_\theta = \frac{C_\theta}{m_f l^2}, \qquad \tilde{C}_\phi = \frac{C_\phi}{m_f l^2}, \qquad \lambda_0 \underline{\Delta} \frac{B}{m_f l^2}, \qquad \lambda_1 \underline{\Delta} \frac{md^2}{m_f l^2}$$

where $()' = \mathrm{d}()/\mathrm{d}\tau$ denotes the differentiation with respect to nondimensional time τ. It has been assumed that $I_1 < I_2 < I_3$; therefore, $0 < r_2 < 1 < r_1$. Notice that the number of moment of inertia parameters has been reduced to two, i.e. r_1 and r_2. Carrying out the above change of variables leads to an equivalent set of dimensionless equations. As will be seen in the following section, these equations must be transformed into the aforementioned form consisting of an unperturbed part (found by discarding higher-order terms; the unperturbed equations are just the equations for a torque-free rigid body) plus a perturbed term in order to apply the Melnikov method. This is done by performing a Taylor expansion of the equations in the powers of perturbation parameter ε and keeping terms up to the appropriate order. The expanded equations can be written as

$$\tilde{h}_1' = \frac{1 - r_1}{r_1} \tilde{h}_2 \tilde{h}_3 - \varepsilon \left[\left(1 + \lambda_0 + \lambda_1 + \frac{\lambda_0 + \lambda_1}{r_1^2} \right) \tilde{h}_2 \tilde{h}_3 - \tilde{h}_3 \cos\phi \cdot \theta' \right] + 0(\varepsilon^2) \tag{13}$$

$$\tilde{h}_2' = \frac{r_1 - r_2}{r_1 r_2} \tilde{h}_1 \tilde{h}_3 - \varepsilon \left[\left(\frac{1 + \lambda}{r_2^2} + \frac{\lambda_0 + \lambda_1}{r_1^2} \right) \tilde{h}_1 \tilde{h}_3 + \frac{\lambda}{r_2} \tilde{h}_3 \alpha' + \frac{\tilde{h}_3}{r_2} \theta' \sin\phi \right] + 0(\varepsilon^2) \tag{14}$$

$$\tilde{h}_3' = \frac{r_2 - 1}{r_2} \tilde{h}_1 \tilde{h}_2 - \varepsilon \left[\left(1 + \lambda_0 + \lambda_1 + \frac{1 + \lambda}{r_2^2} \right) \tilde{h}_1 \tilde{h}_2 + \frac{\lambda}{r_2} \tilde{h}_2 \alpha' + \left(\tilde{h}_1 \cos\phi + \frac{\tilde{h}_2}{r_2} \sin\phi \right) \theta' \right] + 0(\varepsilon^2) \tag{15}$$

$$\alpha'' = -[\tilde{K}/(G_1 r_3)]\alpha + [(r_1 - 1)/(r_1 r_2)]\tilde{h}_2 \tilde{h}_3 +) + O(\varepsilon) \tag{16}$$

$$\theta'' + \tilde{C}_\vartheta \theta' + [(\tilde{\omega}_1 \cos\phi + \tilde{\omega}_2 \sin\phi)(1 - \cos 2\theta) - \tilde{\omega}_3 \sin 2\theta]\phi' - \tfrac{1}{2} \sin 2\theta \cdot \phi'^2 + \sin\phi \cdot \tilde{\omega}_1' - \cos\phi \cdot \tilde{\omega}_2' - \cos 2\theta \cdot (\tilde{\omega}_1 \tilde{\omega}_2 \sin 2\phi + \tilde{\omega}_2 \tilde{\omega}_3 \sin\phi) + \tfrac{1}{2} \sin 2\theta [(\tilde{\omega}_1 \cos\phi + \tilde{\omega}_2 \sin\phi)^2 - \tilde{\omega}_3^2] = 0 \tag{17}$$

$$\phi'' \sin^2\theta + (\theta' \sin 2\theta + \tilde{C}_\phi)\phi' + [(\tilde{\omega}_1 \cos\phi + \tilde{\omega}_2 \sin\phi)(\cos 2\theta - 1) + \tilde{\omega}_3 \sin 2\theta]\theta' + \frac{\tilde{\omega}_1'}{2} \sin 2\theta \cdot \cos\phi + \frac{\tilde{\omega}_2'}{2} \sin 2\theta \cdot \sin\phi + \tilde{\omega}_3' \sin^2\theta + \tilde{\omega}_1 \tilde{\omega}_2 \cos 2\phi \cdot \sin^2\theta + \left(\frac{\tilde{\omega}_2^2}{2} - \frac{\tilde{\omega}_1^2}{2} \right) \sin 2\phi \cdot \sin^2\theta + \frac{\tilde{\omega}_1 \tilde{\omega}_3}{2} \sin 2\theta \cdot \sin\phi - \frac{\tilde{\omega}_2 \tilde{\omega}_3}{2} \sin 2\theta \cdot \cos\phi = 0 \tag{18}$$

For simplicity, in the above derivation, the assumption is made that θ is a small oscillatory component. This assumption permits us to consider only the rotary liquid slosh, which is a reasonable model in the case the attitude dynamics for spinning spacecraft are studied. The nondimensional angular velocity $\tilde{\omega}_i$ can be obtained as follows:

$$\tilde{\omega}_1 = \frac{\tilde{h}_1}{r_2} - \varepsilon \left(\frac{1 + \lambda}{r_2^2} \tilde{h}_1 + \frac{\lambda}{r_2} \alpha' + \frac{\sin\phi}{r_2} \theta' \right)$$
$$\tilde{\omega}_2 = \tilde{h}_2 - \varepsilon [(1 + \lambda_0 + \lambda_1)\tilde{h}_2 + \theta' \cos\phi]$$
$$\tilde{\omega}_3 = \frac{\tilde{h}_3}{r_1} - \frac{\lambda_1 + \lambda_0}{r_1^2} \tilde{h}_3 \varepsilon \tag{19}$$

In the next section, a procedure to reduce Eqs. (13–18) to three equations is described, in which the equations have a spherical unperturbed phase space by the elimination of Eqs. (13–18).

III. Melnikov Method

A. Melnikov Function

To apply the Melnikov method, the unperturbed phase space must have a structure that includes heteroclinic connections between pairs of saddle points or orbits homoclinic to a single saddle point. The Melnikov method will evaluate changes in the Poincaré map of this structure when the system is perturbed. The unperturbed phase space for the system given in Eqs. (13–18) is found by setting $\varepsilon = 0$. Doing so eliminates the dependence of Eqs. (13–15) on Eqs. (16–18) and allows us to solve Eqs. (13–15) independently of Eqs. (16–18). The unperturbed system of equations corresponding to Eqs. (13–15) is given by

$$\tilde{h}_1' = \frac{1 - r_1}{r_1} \tilde{h}_2 \tilde{h}_3 \tag{20}$$

$$\tilde{h}_2' = \frac{r_1 - r_2}{r_2 r_1} \tilde{h}_1 \tilde{h}_3 \tag{21}$$

$$\tilde{h}_3' = \frac{r_2 - 1}{r_2} \tilde{h}_1 \tilde{h}_2 \tag{22}$$

which are identical to the Euler rotational equations of motion for a torque-free rigid body. The phase space for the unperturbed system is a sphere shown in Fig. 3, where the nondimensional body-fixed angular momentum components $\tilde{h}_1$, $\tilde{h}_2$, and $\tilde{h}_3$ are the phase variables. The phase space has six equilibrium points at $\{(\pm 1, 0, 0), (0, \pm 1, 0), (0, 0, \pm 1)\}$, where the equilibrium points $(\pm 1, 0, 0)$ and $(0, 0, \pm 1)$ are neutrally stable centers corresponding to minor and major axis spins, respectively, and the equilibrium points at

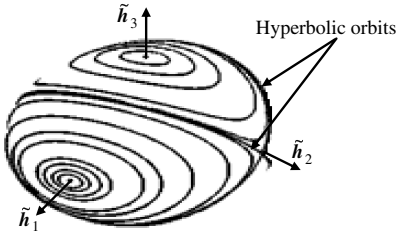

Fig. 3 Momentum sphere illustrating the heteroclinic orbits and the hyperbolic saddle points; curves are orbits of constant energy.

$(0, \pm 1, 0)$ are unstable hyperbolic saddle points corresponding to an intermediate axis spin. Note the presence of heteroclinic orbits jointing the pair of saddle points.

The Melnikov method is now applied to the system of Eqs. (13–18). The Melnikov method is a perturbation technique that gives global information about the system dynamics. The method detects intersections of the stable and unstable manifolds of hyperbolic saddles in planar Poincaré maps. Existence of these intersections implies the existence of Smale horseshoes and chaos via the Smale–Birkhoff theorem (see [12]). For a detailed presentation of the Melnikov theory, see Guckenheimer and Holmes [13] or Wiggins [14,15]. The most common version of the Melnikov method considers systems of the form

$$\dot{\mathbf{x}} = \mathbf{f}(\mathbf{x}; \boldsymbol{\beta}) + \varepsilon \mathbf{g}(\mathbf{x}, \tau; \boldsymbol{\beta}), \qquad x = \begin{Bmatrix} u \\ v \end{Bmatrix} \in \mathbf{R}^2 \tag{23}$$

where g is periodic in τ, $f(x, \beta)$ is a Hamiltonian vector field defined on R^2, and $\varepsilon g(x, \tau, \beta)$ is a small perturbation, which need not be Hamiltonian. The variable $\boldsymbol{x} = (\tilde{h}_1, \tilde{h}_2, \tilde{h}_3, \alpha, \alpha', \theta, \theta', \phi, \phi')$, and β is a vector of system parameters. It would appear that the Melnikov method would not be applicable to our system given the form of the equations in Eq. (23). That is, the Melnikov method applies to systems for which the Poincaré map is planar and the system considered herein is nine-dimensional. On the other hand, close inspection of Eqs. (13–18) reveals that Eqs. (13–15) couple with Eqs. (15–18) only through the perturbation terms in Eqs. (13–15). Therefore, Eqs. (13–15) can be solved for their unperturbed solutions (i.e., the solutions for $\tilde{h}_1$, $\tilde{h}_2$, and $\tilde{h}_3$ with $\varepsilon = 0$) and substitute these solutions into Eqs. (16–18). Then, Eqs. (16–18) are solved for their unperturbed solutions (i.e., the solution for α, θ, and ϕ, with $\varepsilon = 0$) and then substitute the unperturbed solutions for α, θ, and ϕ into the perturbations of Eqs. (13–15). This process results in three nonautonomous equations in $\tilde{h}_1$, $\tilde{h}_2$, and $\tilde{h}_3$, with the unperturbed parts represented by the Euler equation of rotational motion and perturbation terms that are a function of the $\tilde{h}_i$, the system parameters, and time τ. This process of reducing the system to three first-order equations from nine equations still does not admit the application of the planar form of the Melnikov method. However, a result due to Holmes and Marsden [12] allowed the application of the Melnikov method directly to the equations involving $\tilde{h}_1$, $\tilde{h}_2$, and $\tilde{h}_3$. The Melnikov function, as given in [12], can be written as

$$M(\tau_0) = \int_{-\infty}^{\infty} \nabla \tilde{h}[\mathbf{q}_0(\tau)] \cdot \{\mathbf{f}[\mathbf{q}_0(\tau)] + \mathbf{g}[\mathbf{q}_0(\tau), \tau + \tau_0]\}\, \mathrm{d}\tau \tag{24}$$

where $\nabla \tilde{h}$ is the gradient of the Hamiltonian $\tilde{h}$ of the unperturbed system with respect to $\tilde{h}_i$, $\boldsymbol{f}$ is the unperturbed part of the system, $\boldsymbol{g}$ is the $\mathcal{O}(\varepsilon)$ perturbation of the system, and $\boldsymbol{q}_0(\tau)$ is the solution for the heteroclinic orbits or trajectories of the unperturbed system. The nondimensional Hamiltonian for the system is given by $\tilde{h} = (1/2)(\tilde{h}_1^2/r_2 + \tilde{h}_2^2 + \tilde{h}_3^2/r_1)$ and is simply the kinetic energy of the unperturbed system, i.e., of the carrier body. The gradient of $\tilde{h}$ with respect to the body-fixed angular momentum components is thus the vector $\nabla \tilde{h} = \{\tilde{h}_1/r_2,\ \tilde{h}_2,\ \tilde{h}_3/r_1\}$. Because it can be readily shown that $\nabla \tilde{H} \cdot \mathbf{f} = 0$, Eq. (24) can be simplified to

$$M(\tau_0) = \int_{-\infty}^{\infty} \nabla \tilde{H}[\mathbf{q}_0(\tau)] \cdot \mathbf{g}[\mathbf{q}_0(\tau), \tau + \tau_0]\, \mathrm{d}\tau \tag{25}$$

Before the integral in Eq. (25) can be evaluated, solutions $q_0(\tau)$ must be found along the heteroclinic orbits of the unperturbed system given by Eqs. (20–22) and find the unperturbed solution to Eqs. (16–18) so that α', $\sin\phi$, $\cos\phi$, and θ' may be substituted into the perturbation terms of Eqs. (13–15).

The solution along the heteroclinic orbits can be found in terms of hyperbolic trigonometric functions (see [1]). These solutions are given as follows:

$$\tilde{h}_1 = s_1 X_1 \sec h(d\tau) \tag{26}$$

$$\tilde{h}_2 = s_2 \tanh(d\tau) \tag{27}$$

$$\tilde{h}_3 = s_3 X_3 \sec h(d\tau) \tag{28}$$

where $X_1 \equiv \sqrt{r_2(1 - r_1)/(r_2 - r_1)}$, $X_3 \equiv \sqrt{r_1(r_2 - 1)/(r_2 - r_1)}$, $D \equiv \sqrt{(r_1 - 1)(1 - r_2)/(r_1 r_2)}$, and $\{s_1, s_2, s_3\} = \pm 1$ such that the product $s_1 s_2 s_3 = 1$ (these permutations give all four of the heteroclinic orbits shown in Fig. 3).

Keeping in mind the assumption that θ is a small oscillatory component, the expressions for $\sin\phi$, $\cos\phi$, and θ' can be obtained from Eqs. (17) and (18) with $\varepsilon = 0$:

$$\sin\phi = \frac{\tilde{\omega}_2\tilde{\omega}_3 - \tilde{\omega}_1'}{\sqrt{(\tilde{\omega}_2' + \tilde{\omega}_1\tilde{\omega}_3)^2 + (\tilde{\omega}_2\tilde{\omega}_3 - \tilde{\omega}_1')^2}} \tag{29}$$

$$\cos\phi = \frac{\tilde{\omega}_2' + \tilde{\omega}_1\tilde{\omega}_3}{\sqrt{(\tilde{\omega}_2' + \tilde{\omega}_1\tilde{\omega}_3)^2 + (\tilde{\omega}_2\tilde{\omega}_3 - \tilde{\omega}_1')^2}} \tag{30}$$

$$\theta' = \frac{1 - r_1 - r_2}{2r_2}\tilde{h}_2 \cos\phi + \frac{2r_1 - r_2}{2r_2}\tilde{h}_1 \sin\phi \tag{31}$$

In deriving Eq. (31), the fact that the angular momentum for ϕ is constant is used, i.e., $\mathrm{d}(m_f l^2 \sin^2\theta \cdot \phi)/\mathrm{d}t = 0$ [26].

Equation (16) can be solved, with $\varepsilon = 0$, for α by substituting in the unperturbed solutions for $\tilde{h}_2$ and $\tilde{h}_3$. The approximate solution to this equation is derived by Miller and Gray [17] to be $\alpha = A \sin(\Omega\tau + \Phi)$, where the square of the amplitude A is given by

$$A^2 = \left[\alpha_0 - \frac{\pi C}{2D^2}\sec\frac{\pi\Omega}{2D}\right]^2 + \left\{\frac{\alpha_0'}{\Omega} + \frac{C_1}{\Omega D} + \frac{C_1}{2D^2}\left[\pi\tanh\frac{\pi\Omega}{2D} + i\Psi\left(\frac{D + i\Omega}{4D}\right) - i\Psi\left(\frac{D - i\Omega}{4D}\right)\right]\right\}^2 \tag{32}$$

The tangent of the phase angle Φ is given by

$$\tan\Phi = \left[\alpha_0 - \frac{\pi C_1}{2D^2}\sec h\frac{\pi\Omega}{2D}\right] \Bigg/ \left\{\frac{\alpha_0'}{\Omega} + \frac{C_1}{\Omega D} + \frac{C_1}{2D^2}\left[\pi\tanh\frac{\pi\Omega}{2D} + i\Psi\left(\frac{D + i\Omega}{4D}\right) - i\Psi\left(\frac{D - i\Omega}{4D}\right)\right]\right\} \tag{33}$$

where α_0 is the initial angle of twist of the torsional appendage, α_0' is the initial twist rate, Ω is the frequency of appendage oscillation defined by $\Omega \equiv \sqrt{\tilde{K}/(\lambda_1 G_1 r_3)}$, C_1 is defined by

$$C_1 \equiv \frac{r_1 - 1}{r_1 r_2}\sqrt{\frac{r_1(1 - r_2)}{r_1 - r_2}} \tag{34}$$

and $\Psi = \Psi(z)$ is the Euler digamma function defined for complex variables as follows:

$$\Psi(z) = \int_0^{\infty}\left[e^{-\tau} - \frac{1}{(1 + \tau)^z}\right]\frac{\mathrm{d}\tau}{\tau}, \qquad R(z) > 0 \tag{35}$$

In accordance with the Melnikov method, τ is now replaced by $\tau + \tau_0$ everywhere that τ appears explicitly. Then the resulting expression for $\sin\phi$, $\cos\phi$, θ', and α' is substituted into Eqs. (13–15) to obtain the final form of the Melnikov integration. The Melnikov integral given in Eq. (25) is now expanded, and the unperturbed solutions in Eqs. (26–28), along the heteroclinic orbits, are substituted for $\tilde{h}_1$, $\tilde{h}_2$, and $\tilde{h}_3$ in the integral. Because the integral is performed over the interval $(-\infty, \infty)$, all odd functions in the integrand can be eliminated, leaving the following terms in the Melnikov integral:

Downloaded by University of Hong Kong Libraries on October 21, 2012 | http://arc.aiaa.org | DOI: 10.2514/1.J050144

$$M(\tau_0) = \int_{-\infty}^{\infty} \left(\frac{1 + r_1 - r_2}{C_\vartheta r_1 r_2^2} X_1^2 X_3^2 \mathrm{Sec}^4 D\tau + \frac{r_1 + r_2 - 1}{C_\vartheta r_1 r_2^2} X_3^2 \tanh^2 D\tau \cdot \sec h^2 D\tau + \frac{1 + r_1 - r_2}{C_\vartheta r_1^2 r_2} X_1 X_3^2 \sec h^3 D\tau \right) \mathrm{d}\tau - \int_{-\infty}^{+\infty} \left(\frac{r_1 + 1}{r_1 r_2} \lambda A \Omega X_3 \sec hD\tau \cdot \tanh D\tau \cdot \sin \Omega\tau \cdot \sin \Omega\tau_0 \right) \mathrm{d}\tau \tag{36}$$

The integrals in Eq. (36) can be evaluated symbolically with the software Mathematica. After integrating, the Melnikov function is arrived at for the following system of equations:

$$M(\tau_0) = \frac{\pi}{D}(r_1 + 1)\lambda A \Omega^2 \sec h \frac{\pi\Omega}{2D} \cdot \sin \Omega\tau_0 - \frac{X_3^2}{C_\vartheta r_1 r_2} \left[(1 + r_1 - r_2) X_1 \left(\frac{4}{3} r_1 X_1 + \frac{\pi}{2} r_2 \right) + \frac{2}{3}(r_1 + r_2 - 1)(r_1 + 1) \right] \tag{37}$$

Because the Melnikov function is a measure of distance between stable and unstable manifolds in the Poincaré map of the system, zeros of the Melnikov function indicate intersections of the two manifolds. The function contains two terms, one of which is constant and the other which varies sinusoidally with τ_0. Zeros of this function will occur wherever the amplitude of the sinusoidal terms is greater than the constant term. The Melnikov criterion becomes

$$\frac{\pi}{D}(r_1 + 1)\lambda A \Omega^2 \sec h \frac{\pi\Omega}{2D} \geq \frac{X_3^2}{C_\vartheta r_1 r_2} \left[(1 + r_1 - r_2) X_1 \times \left(\frac{4}{3} r_1 X_1 + \frac{\pi}{2} r_2 \right) + \frac{2}{3}(r_1 + r_2 - 1)(r_1 + 1) \right] \tag{38}$$

This criterion is valid, provided that the perturbation parameter ε is sufficiently small.

B. Results Based on the Melnikov Method

The derived analytical criterion in the previous section can be used to find chaotic and nonchaotic regions in parameter space and, if necessary, avoid chaotic motion in this class of satellite systems. Inspection of Eq. (38) reveals that the Melnikov criterion is a function of five nondimensional system parameters (r_1, r_2, λ, $\tilde{\Omega}$, and $\tilde{C}_\theta$). Three-dimensional parameter subspaces are investigated by choosing the values of three of the parameters and then plotting the other three. Parametric studies of the three-dimensional parameter subspace for Eq. (38) are shown in Figs. 4–8. In these figures, values of the parameters above the surface correspond to chaotic attitude motion. These analytical results will eventually need to be compared with numerical experiments, but the numerical experiments have turned out to be too numerous and extensive to be presented here, and some typical examples of the numerical simulations will be presented in the next section.

Figure 4 shows the dividing surface between chaotic and nonchaotic motions in $\lambda - \tilde{\Omega} - \tilde{C}_\theta$ space as determined by Eq. (38). The values of the movement of inertia parameters were chosen to be $r_1 = 1.3$ and $r_2 = 0.6$. The values of the parameters above the surface are chaotic. The surface flattens out at $\tilde{C}_\theta = 1$ since $\tilde{C}_\theta < 1$ is imposed. The surface shows the dependence of the criterion for chaos on fuel fraction and frequency of motion of the appendage. It is seen that values of smaller values of $\tilde{\Omega}$ display large regions of chaotic behavior because of the very likely easy coupling between the fuel slosh of low frequency and the flexible appendage in these cases. It is obvious that increasing values of λ will enlarge the regions of chaotic behavior. This result shows the stronger interaction between the appendage and fuel slosh will result in more chaos because λ is a measure of appendage size relative to the fuel slosh mass.

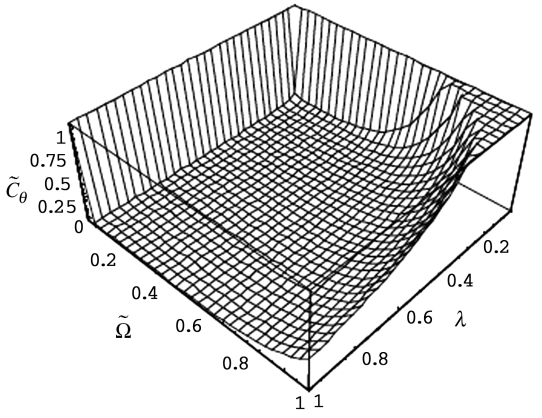

Fig. 4 Surface separating chaotic from nonchaotic motions.

Figure 5 shows the dividing surface between chaotic and nonchaotic motions in $r_2 - \lambda - \tilde{C}_\theta$ space as determined by Eq. (38). The value of the movement of inertia parameters was chosen to be $r_1 = 1.5$, and the frequency $\tilde{\Omega}$ of the flexible appendage is chosen to be 0.69. The surface shows the dependence of the criterion for chaos on the shape of the rigid body, the fraction of fuel slosh, and the size of the appendage. It is seen that, for a value of $r_2 \to 1$, which corresponds to a nearly symmetric oblate body, no chaotic motion occurs. Increasing λ will produce a larger region of chaos in parameter space.

Figure 6 shows the dividing surface between chaotic and nonchaotic motions in $r_1 - \lambda - \tilde{C}_\theta$ space as determined by Eq. (38). The value of movement of the inertia parameters was chosen to be $r_2 = 0.7$, and the frequency $\tilde{\Omega}$ of the flexible appendage is chosen to be 1.2. This plot shows a similar chaotic behavior in dependence on the system parameters, as in Fig. 5, except that it is impossible to obtain chaos as the value of $r_1 \to 1$. That is, chaos is very difficult to achieve for a prolate body.

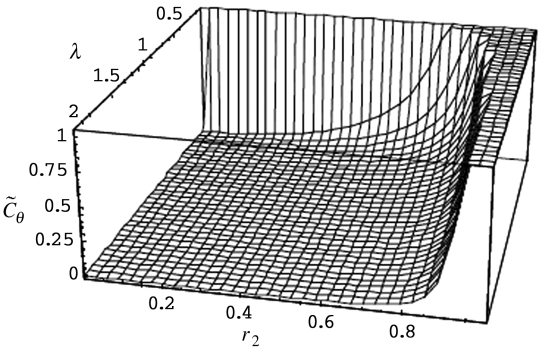

Fig. 5 Surface separating chaotic from nonchaotic motions.

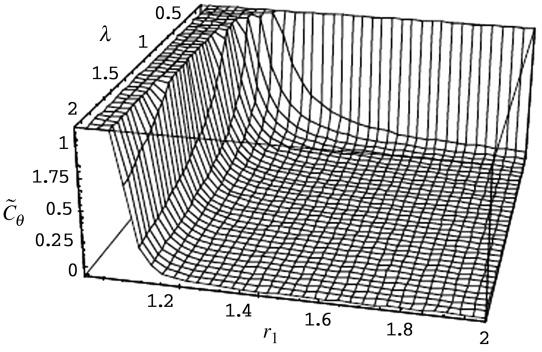

Fig. 6 Surface separating chaotic from nonchaotic motions.

Downloaded by University of Hong Kong Libraries on October 21, 2012 | http://arc.aiaa.org | DOI: 10.2514/1.J050144

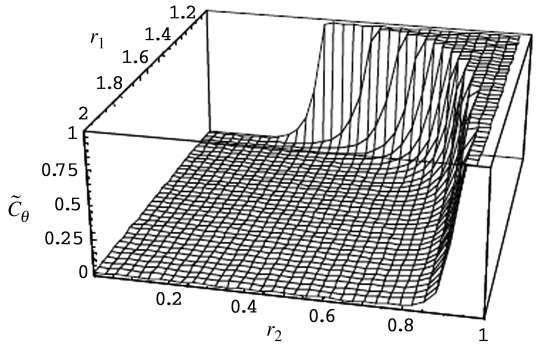

Fig. 7 Surface separating chaotic from nonchaotic motions.

Figure 7 shows the dividing surface between chaotic and nonchaotic motions in $r_1 - r_2 - \tilde{C}_\theta$ space as determined by Eq. (38). The surface shows the dependence of the criterion for chaos on fuel fraction. The parameters $\tilde{\Omega}$ and λ are fixed at the same value of 1.2. It is evident that, as the carrier's body shape parameters approach two opposite limiting shapes r_1 or $r_2 \to 1$, chaos is very difficult to achieve.

Figure 8 shows the dividing surface between chaotic and nonchaotic motions in $r_2 - \tilde{\Omega} - \tilde{C}_\theta$ space as determined by Eq. (38). The body shape parameter and the ratio of the mass movement of inertia of the appendage to fuel slosh are chosen to be the same value as 1.5. It is again seen that, for an oblate body shape, as $r_2 \to 1$, the chaos is more difficult to achieve. Increasing the value of the appendage frequency parameter $\tilde{\Omega}$ has the effect of suppressing the chaos. Figure 8 also presents an interesting phenomenon that the chaotic motion is virtually assured for values of r_2 approaching unity and small values of $\tilde{\Omega}$. This result is not obvious in a physically realistic sense and is a subject for further study.

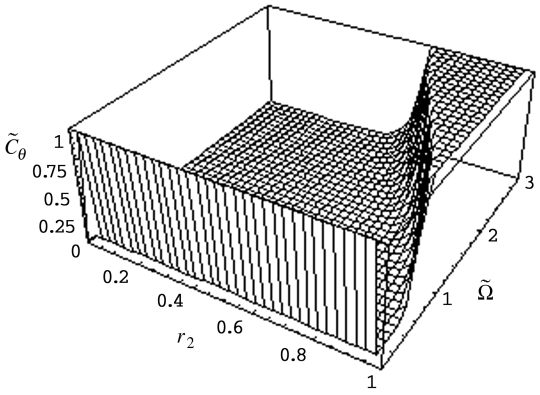

Fig. 8 Surface separating chaotic from nonchaotic motions.

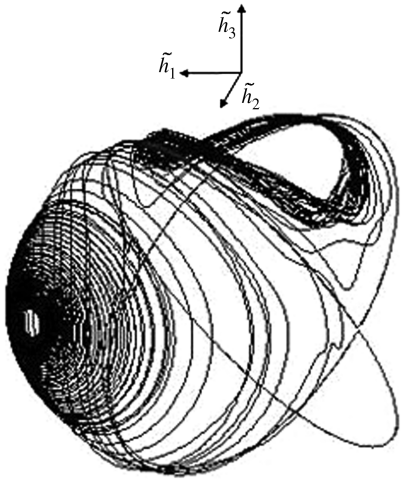

Fig. 9 Path of the angular momentum vector starts with a positive minor axis spin and finishes with a positive major axis spin with anomaly nutation or large limit cycle.

IV. Numerical Simulation

To check the range of the validity of the Melnikov result, extensive numerical simulations are carried out and representative examples of the results of some of the numerical simulations are shown from Figs. 9–14. In all simulations discussed herein, each trajectory is shown on the surface of the momentum sphere in $\tilde{h}_1 - \tilde{h}_2 - \tilde{h}_3$ space, and the two great circles passing through the $\tilde{h}_2$ axis are the unperturbed heteroclinic cycles. Each simulation starts with the following initial conditions:

$$y_0 = [\cos(\pi/36), \sin(\pi/36), 0, 0, 0, 0.1, 0, 0.2, 0]$$

The values of the system parameters used to generate all of the trajectories obtained by simulating Eqs. (13–18) may be found in Table 1. In the case of no external forcing movement, the viscous fuel

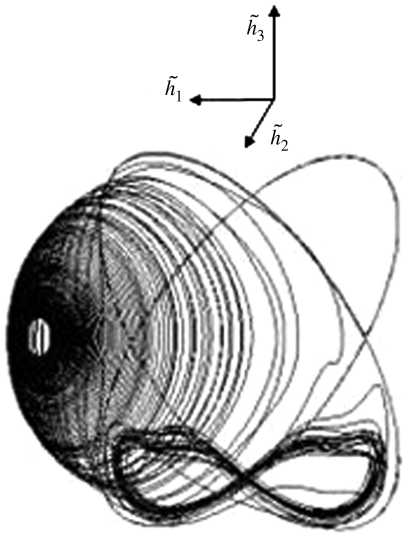

Fig. 10 Path of the angular momentum vector starts with a negative minor axis spin and finishes with a negative major axis spin with anomaly nutation or large limit cycle.

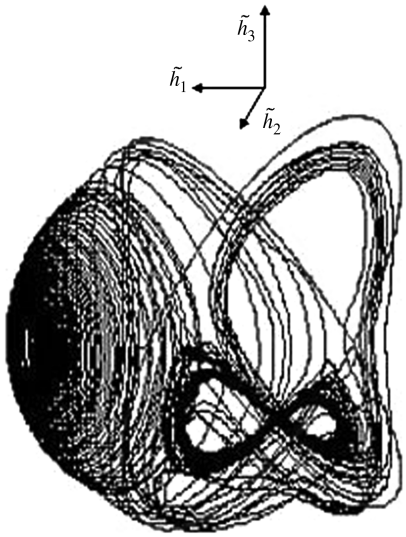

Fig. 11 Path of the angular momentum vector starts with a positive minor axis spin undergoing unstable limit cycle and finishes with a stable limit cycle.

Downloaded by University of Hong Kong Libraries on October 21, 2012 | http://arc.aiaa.org | DOI: 10.2514/1.J050144

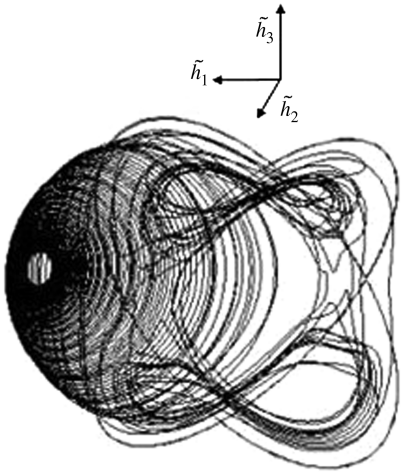

Fig. 12 Path of the angular momentum vector starts with a positive minor axis spin and finishes with a double large limit cycle around major axis.

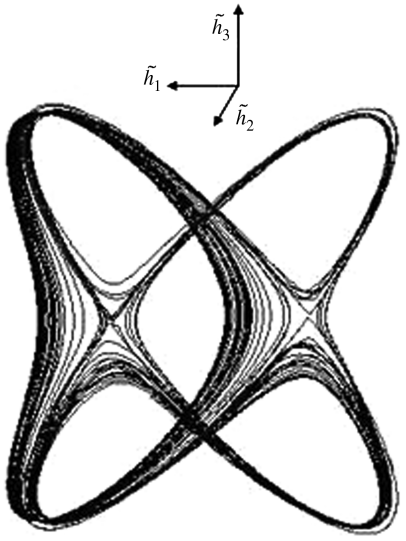

Fig. 13 Path of the angular momentum vector starts with a positive minor axis spin and finishes with a quasi-periodic trajectory of many excurses between two hyperbolic saddles.

slug provides the energy dissipation. Dynamic energy T decreases, and the energy ellipsoid shrinks with time. This leads to an open polhode path that spirals outward from the minor axis and captures on the major axes, as shown in Fig. 9. As shown clearly in Fig. 9, the path of the angular of momentum vector in the body axis coordinates starts with a positive minor axis spin and finishes with a positive major axis spin. It is also seen that the trajectory finishes with a spin

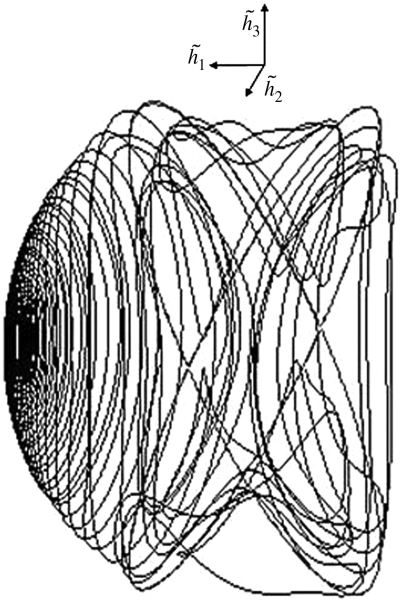

Fig. 14 Path of the angular momentum vector in body axis coordinates starts with a positive minor axis spin and finishes with chaotic spin.

about the major axis with a large amount of nutation or a large limit cycle due to the negative effect of fuel slosh on the spacecraft attitude maneuver, which means that the spacecraft must be stabilized by active control to force it to finish the reorientation maneuver or spin transition. Similarly, a negative minor axis spin with a large limit cycle is shown in Fig. 10. A numerical experiment reveals that the orientation of the spacecraft relative to the inertially fixed angular momentum vector at the end of the maneuver cannot be determined a priori. The spacecraft can end up with either a positive or a negative major axis spin. Physically, this corresponds to two final attitudes that are 180 deg apart. In Fig. 11, the trajectory represents a transient unstable limit cycle around the intermediate axis and a final steady-state limit cycle around the negative major axis. Figure 12 shows the double limit cycles around the positive major axis and negative major axis.

As can be seen in Fig. 13, the numerical result shows that the spacecraft motion ends up with the final limit cycle in coalescence with heteroclinic orbits. In Fig. 13, the beginning outward spiral part of the orbit around the positive minor axis is not shown to better highlight the final structure of the orbits. This simulation result corresponds to an orbit connecting a periodic orbit and a heteroclinic or homoclinic orbit. This simulation result reveals a complex nonlinear behavior in the bifurcation process of heteroclinic orbits. It seems that the similarity between periodic (or Hopf) and heteroclinic bifurcations will in fact become more than a superficial analogy. Heteroclinic orbits can be viewed as limits of nearby periodic orbits. Numerical results confirm the existence of periodic and heteroclinic orbits cascading to a saddle center at isolated parameter values, which gives rise to multiplicity and shift dynamics in the nonlinearly

Table 1 Parameters used to generate trajectories in numerical simulations

Parameters	Figure 9	Figure 10	Figure 11	Figure 12	Figure 13	Figure 14
r_1	1.5	1.5	1.5	1.5	1.5	1.5
r_2	0.6	0.6	0.8	0.6	0.6	0.6
r_3	1.5	1.5	1.5	1.87	1.5	1.87
$\tilde{K}$	2.5	1.5	1.5	0.95	1.5	0.8
ε	0.02	0.02	0.02	0.02	0.02	0.02
G_1	1.5	1.5	0.8	1.5	1.8	1.5
$\tilde{C}_\theta$	0.85	0.85	0.95	0.95	0.95	0.85
$\tilde{C}_\phi$	0.52	0.52	0.52	0.52	0.52	0.52
λ	1.45	1.45	1.0	1.45	1.45	1.45
λ_0	0.5	0.5	1.5	0.5	0.5	0.5
λ_1	1.5	1.5	1.5	1.5	1.5	1.5

Downloaded by University of Hong Kong Libraries on October 21, 2012 | http://arc.aiaa.org | DOI: 10.2514/1.J050144

coupling system. It is worthwhile to make clear the physical implications behind this nonlinear phenomenon. Perhaps some more comprehensively numerical tests are necessary in the near future to further verify this new kind of heteroclinic bifurcation. Figure 14 shows a trajectory eventually ending up with a chaotic orbit. It is readily seen that the trajectory does not settle down into a regular pattern.

In the above numerical simulations, it is revealed that the Melnikov surface produced from the Melnikov analytical criterion tends to bound those regions of parameter space exhibiting not only chaotic dynamics but also some other complicated bifurcation dynamics, demonstrating the richness of nonlinear dynamics inherent in the liquid-filled flexible spacecraft. It is useful to note that, because of the high dimension of the parameter space, it is prohibitive to study thoroughly the phase spaces in detail, so some parameters have been chosen that the author feels are of fundamental importance to the system. The trajectories shown in the numerical simulation results represent six of a myriad of other types of trajectories that have been numerically discovered in this system. In addition, all the data used in producing trajectories in the figures shown above are chosen according to the Melnikov criterion.

Downloaded by University of Hong Kong Libraries on October 21, 2012 | http://arc.aiaa.org | DOI: 10.2514/1.J050144

V. Conclusions

In this paper, the nine-dimensional ordinary differential equations governing the attitude motion of the partially liquid-filled spacecraft with a flexible appendage are derived and transformed into a form suitable for the application of the Melnikov method. The coupled slosh–spacecraft with a flexible appendage in attitude maneuver carrying a sloshing liquid is considered as a multibody system with the sloshing motion modeled as a spherical pendulum. By using the Melnikov integral, the theoretical criterion for the chaotic attitude motion of the spacecraft is obtained. In addition, the subspace of the full-parameter space is studied analytically and numerically to obtain a qualitative and quantitative understanding of the interaction of the various parameters leading to nonlinear motion. From the analytical and numerical results, it is shown that the onset of chaotic dynamics is, in general, strongly linked to the shape of the rigid body, the viscosity of the liquid fuel, the fraction of the fuel slosh mass, the size of the flexible appendage, and the torsional stiffness of the flexible appendage. From the numerical results, it is seen that the partially liquid-filled satellite with a flexible appendage possesses many random characteristics of a nonperiodic solution that are theoretically proved to be chaotic by using the Melnikov method. It is concluded that the Melnikov criterion not only gives a prediction for chaotic attitude motion but also gives a prediction for some other spacecraft attitude motion, such as periodic limit cycle, coalescence between heteroclinic orbit and periodic orbit, heteroclinic orbit bifurcation, etc. It is also worthy of note that the spacecraft model studied in this paper can exhibit chaos resulting from the inherent flexibility of its components and intrinsic nonlinearity of rotary fuel slosh but not from the nonautonomous periodic forcing term, which is not presented in the equations system. The analytic criterion and the numerical simulation presented here thus give a useful design tool for spacecraft engineers to avoid potentially chaotic dynamics in the liquid-filled spacecraft system with flexible appendages.

Acknowledgments

The author gratefully acknowledges funding by the Natural Science Foundation of China (10772026 and 11072030), the Ph.D. Programs Foundation of the Ministry of Education of China (20080070011), the Scientific Research Foundation of the Ministry of Education of China for Returned Scholars (20080732040), and the Program of the Beijing Municipal Key Discipline Construction.

References

[1] Adams, G. J., "Dual-Spin Spacecraft Dynamics During Platform Spin-Up," *Journal of Guidance, Control, and Dynamics*, Vol. 3, 1980, pp. 29–36. doi:10.2514/3.55943

[2] Cochran, J. E., and Hkolloway, H. E., "Resonance in the Attitude Motions of Asymmetric Dual-Spin Spacecraft," *Journal of the Astronautical Sciences*, Vol. 28, 1980, pp. 231–254.

[3] Gebman, J. R., and Mingori, D. L., "Perturbation Solution for the Flat Spin Recovery of a Dual-Spin Spacecraft," *AIAA Journal*, Vol. 14, 1976, pp. 859–867. doi:10.2514/3.61428

[4] Hall, C. D., and Rand, R. H., "Spin-Up Dynamics of Axial Dual-Spin Spacecraft," *Journal of Guidance, Control, and Dynamics*, Vol. 17, 1994, pp. 30–37. doi:10.2514/3.21155

[5] Or, A. C., "Resonances in the Design Dynamics of Dual-Spin Spacecraft," *Journal of Guidance, Control, and Dynamics*, Vol. 14, 1991, pp. 321–329. doi:10.2514/3.20643

[6] Barba, P. M., Furumoto, N., and Leliakov, I. P., "Techniques for Flat-Spin Recovery of Spinning Satellites," AIAA Guidance and Control Conference, Key Biscayne, FL, AIAA Paper 1973-0859, 1973.

[7] Tong, X., and Tabarrok, B., "Bifurcation of Self-Excited Rigid Bodies Subjected to Small Perturbation Torques," *Journal of Guidance, Control, and Dynamics*, Vol. 20, 1997, pp. 123–128. doi:10.2514/2.4004

[8] Cooper, J. H., and Bishop, R. H., "Chaos in Rigid Body Attitude Dynamics," AIAA Paper 1999-3970, 1999.

[9] Meehan, P. A., and Asokanthan, S. F., "Chaotic Motion in a Rotating Body with Internal Energy Dissipation," *Nonlinear Dynamics and Stochastic Mechanics*, edited by W. H. Kliemann, W. F. Alangford, and N. S. Namachchivaya, American Mathematical Soc., Providence, RI, 1996, pp. 175–205.

[10] Meehan, P. A., and Asokanthan, S. F., "Control of Chaotic Motion in a Spinning Spacecraft with a Circumferential Nutation Damper," *Nonlinear Dynamics*, Vol. 17, 1998, pp. 269–284. doi:10.1023/A:1008274705245

[11] Meehan, P. A., and Asokanthan, S. F., "Analysis of Chaotic Instability in a Rotating Body with Internal Energy Dissipation," *International Journal of Bifurcation and Chaos in Applied Sciences and Engineering*, Vol. 16, 2006, pp. 1–19. doi:10.1142/S021812740601454X

[12] Holmes, P. J., and Marsden, J. E., "Horseshoes and Arnold Diffusion for Hamiltonian Systems on Lie Groups," *Indiana University Mathematics Journal*, Vol. 32, 1983, pp. 273–309. doi:10.1512/iumj.1983.32.32023

[13] Guckenheimer, J., and Holmes, P., *Nonlinear Oscillations, Dynamical Systems, and Bifurcations of Vector Fields*, Spring–Verlag, New York, 1983.

[14] Wiggins, S., *Global Bifurcations and Chaos*, Springer–Verlag, New York, 1998, pp. 184–204.

[15] Wiggins, S., *Introduction to Applied Nonlinear Dynamics Systems and Chaos*, Springer–Verlag, New York, 1990, pp. 396–416.

[16] Gray, G. L., Dobson, L., and Kammer, D. C., "Chaos in a Spacecraft Attitude Maneuver Due to Time-Periodic Perturbations," *Journal of Applied Mechanics*, Vol. 63, 1996, pp. 501–508. doi:10.1115/1.2788896

[17] Miller, A. J., and Gray, G. L., "Nonlinear Spacecraft Dynamics with a Flexible Appendage, Damping, and Moving Internal Submasses," *Journal of Guidance, Control, and Dynamics*, Vol. 24, 2001, pp. 605–615. doi:10.2514/2.4752

[18] Rumyantsev, V. V., "On the Lyapunov'S Methods in the Study of Stability of Motions of Rigid Bodies with Fluid-Filled Cavities," *Advances in Applied Mechanics*, Vol. 8, 1964, pp. 183–232. doi:10.1016/S0065-2156(08)70355-7

[19] Rahn, C. D., "Reorientation Maneuver for Spinning Spacecraft," *Journal of Guidance, Control, and Dynamics*, Vol. 14, 1991, pp. 724–728. doi:10.2514/3.20705

[20] Yue, B.-Z., "Heteroclinic Bifurcations in Completely Liquid-Filled Spacecraft with Flexible Appendage," *Nonlinear Dynamics*, Vol. 51, 2008, pp. 317–327. doi:10.1007/s11071-007-9213-6

[21] Yue, B.-Z., "Chaotic Attitude Maneuvers in Spacecraft with a Completely Liquid-Filled Cavity," *Journal of Sound and Vibration*, Vol. 302, 2007, pp. 643–656. doi:10.1016/j.jsv.2006.11.035

[22] Yue, B.-Z., "Chaotic Attitude and Reorientation Maneuver for Completely Liquid-Filled Spacecraft with Flexible Appendage," *Acta Mechanica Sinica (English Edition)*, Vol. 25, 2009, pp. 271–277. doi:10.1007/s10409-008-0213-7

[23] Ibrahim, R. A., and Pilipchuk, V. N., "Recent Advances in Liquid

Sloshing Dynamics," *Applied Mechanics Reviews*, Vol. 54, 2001, pp. 133–199.
doi:10.1115/1.3097293

[24] Nichkawde, C., Harish, P. M., and Ananthkrishnan, N., "Stability Analysis of A Multi-Body System Model for Coupled Slosh-Vehicle Dynamics," *Journal of Sound and Vibration*, Vol. 275, 2004, pp. 1069–1083.
doi:10.1016/j.jsv.2003.07.009

[25] Kana, D. D., "A Model for Nonlinear Rotary Slosh in Propellant Tanks," *Journal of Spacecraft and Rockets*, Vol. 24, 1987, pp. 169–177.
doi:10.2514/3.25891

[26] Kana, D. D., "A Validated Spherical Pendulum Model for Rotary Liquid Slosh," *Journal of Spacecraft and Rockets*, Vol. 26, 1989, pp. 188–196.
doi:10.2514/3.26052

[27] Abramson, H. N., "Dynamics of Contained Liquids: A Personal Odyssey," *Applied Mechanics Reviews*, Vol. 56, 2003, pp. R1–R7.
doi:10.1115/1.1511517

[28] Dodge, F. T., and Abramson, H. N., "Liquid Propellant Dynamics in the SATURN/APOLLO Vehicles: A Look Back," AIAA Paper 2000-1676, 2000.

R. Ohayon
Associate Editor

Downloaded by University of Hong Kong Libraries on October 21, 2012 | http://arc.aiaa.org | DOI: 10.2514/1.J050144